Applied Physics Letters

Low power optical bistability from quantum dots in a nanobeam photonic crystal cavity

Cite as: Appl. Phys. Lett. **121**, 081104 (2022); https://doi.org/10.1063/5.0098003
Submitted: 04 May 2022 • Accepted: 28 July 2022 • Published Online: 22 August 2022

Mustafa Atabey Buyukkaya, Chang-Min Lee, Ahmad Mansoori, et al.

AIP Publishing

Applied Physics Letters ARTICLE scitation.org/journal/apl

Low power optical bistability from quantum dots in a nanobeam photonic crystal cavity

Cite as: Appl. Phys. Lett. **121**, 081104 (2022); doi: 10.1063/5.0098003
Submitted: 4 May 2022 · Accepted: 28 July 2022 ·
Published Online: 22 August 2022

Mustafa Atabey Buyukkaya,[1] Chang-Min Lee,[1] Ahmad Mansoori,[2] Ganesh Balakrishnan,[2] and Edo Waks[1,3,a)]

AFFILIATIONS

[1]Department of Electrical and Computer Engineering and Institute for Research in Electronics and Applied Physics, University of Maryland, College Park, Maryland 20742, USA
[2]Center for High Technology Materials, University of New Mexico, Albuquerque, New Mexico 87106, USA
[3]Joint Quantum Institute, University of Maryland, National Institute of Standards and Technology, College Park, Maryland 20742, USA

[a)]**Author to whom correspondence should be addressed:** edowaks@umd.edu

ABSTRACT

We demonstrate a low power thermally induced optical bistability at telecom wavelengths and room temperature using a nanobeam photonic crystal cavity embedded with an ensemble of quantum dots. The nanobeam photonic crystal cavity is transfer-printed onto the edge of a carrier chip for thermal isolation of the cavity with an efficient optical coupling between the nanobeam waveguide and optical setup. Reflectivity measurements performed with a tunable laser reveal the thermo-optic nature of the nonlinearity. A bistability power threshold as low as 23 μW and an on/off response contrast of 6.02 dB are achieved from a cavity with a moderately low quality factor of 2830. Our device provides optical bistability at power levels an order of magnitude lower than previous quantum-dot-based devices.

Optical bistability is a widely studied nonlinear phenomenon characterized by hysteresis in output light intensity from incident light on a photonic medium.[1] It has been proposed for use in various applications such as optical switches,[2] memories,[3] and differential amplifiers[4] that utilize two stable electromagnetic states in the hysteresis of output light intensity. Large-scale integration of such applications requires optical nonlinearity at low power levels, sufficient modulation speeds, and photonic designs with small footprints that can be integrated with silicon photonic circuits.[5] To achieve some of these requirements, different photonic platforms have been used to demonstrate low power optical bistability, including slab waveguide gratings,[6] photonic crystal cavities,[7] micropillars,[8] and microring resonators[9] using various nonlinear media such as saturable absorbers,[10] Kerr nonlinearities,[11] and thermo-optic materials.[12–14] Among them, thermo-optic devices rely on thermally induced refractive index change, which results from heating in the medium due to optical absorption. This requires materials with high absorption coefficients and strong thermo-optic effects to realize low power optical bistability. It has been shown that the power threshold for thermally induced optical bistability can be reduced by incorporating an absorptive medium to nanophotonic architectures that have strong light and heat confinement in a small mode-volume.[15–19]

Semiconductor quantum dots are promising candidates as an absorptive medium for generating thermally induced optical bistability. They exhibit high absorption coefficients that can efficiently convert light to heat.[12,20] They are grown embedded in a dielectric substrate, which can be lithographically patterned into nanophotonic designs that can enhance optical nonlinearities from quantum dots.[8,12,21,22] They have strong free carrier confinement with a small diffusion length,[23] which can increase the rate of thermal escape of carriers inside the small mode-volume of nanocavities. The previous realizations of optical bistability using quantum dots have been demonstrated in micropillar cavities[8] and 2D photonic crystal cavities.[12] However, these realizations failed to enhance the thermo-optical properties of quantum dots by either suppressing the thermal effects in cryogenic cooling[8] or relying on poor thermal isolation in 2D photonic crystal cavities,[12] which resulted in much higher power thresholds for optical bistability compared to other materials.[18] On the other hand, 1D photonic crystal nanocavities were used to demonstrate thermally induced optical bistability in silicon at power levels as low as a few microwatts due to efficient confinement of light and heat in a small mode-volume.[18] A better light and heat confinement can substantially improve thermo-optical nonlinearities from nanocavities with quantum dots.

In this work, we experimentally demonstrate a quantum-dot-based, thermally induced optical bistability with a power threshold as low as 23 μW. We achieve the low-power optical bistability by embedding quantum dots in an air-suspended nanobeam photonic crystal cavity, which enables both optical and thermal confinement in a small region. We verify the thermal nature of the optical bistability through the reflectivity measurements at different incident powers. Our device works at room-temperature and operates at telecom wavelengths, making it an ideal candidate for a compact and efficient optical nonlinear platform with the potential for hybrid integration with silicon photonics.

Figure 1 illustrates the design for nanobeam photonic crystal cavity. The device consists of a one-dimensional air-cladded GaAs nanobeam photonic crystal cavity with an adiabatic waveguide taper in one side for outcoupling to an objective lens [Fig. 1(a)]. The cavity is realized by tapering and shifting inner 12 holes between two outer photonic crystal mirrors using finite-difference time-domain (FDTD) simulations. The number of mirror holes on the right mirror segment, N_R, is reduced up to 4 to enable light to couple into the cavity from one-side. The number of mirror holes on the left mirror segment, N_L, is kept at 9 to be fully reflective toward the tapered side of the nanobeam waveguide. For $N_R = 4$, simulated quality factor for the cavity resonance at 1280 nm is 229 250. Figure 1(b) shows the fundamental mode profile of the cavity and the Gaussian far field mode profile from the nanobeam taper. Fundamental mode profile shows that mode volume is confined in a small region of $\sim 0.6 \times (\frac{\lambda}{n})^3$. The adiabatic taper at the end of nanobeam waveguide is designed to have a Gaussian mode profile in far field simulation for efficient coupling to an objective lens. Far field mode profile has a coupling efficiency over 90% to the objective lens with a numerical aperture (NA) of 0.7 depicted as white dashed lines in Fig. 4(b).

To realize the proposed device, we used a hybrid fabrication approach. First, we fabricated arrays of nanobeam cavities on a suspended GaAs membrane embedded with InAs quantum dots. This process starts with an InAs/GaAs quantum dot wafer that is grown by molecular beam epitaxy. The wafer consists of three layers of InAs quantum dots embedded in a 200 nm thick GaAs membrane on top of a 1 μm thick AlGaAs sacrificial layer. Each layer of quantum dots has a density of $1 \times 10^{10}\,\mathrm{cm}^{-2}$, and room temperature photoluminescence of quantum dots is centered around 1280 nm with a 60 nm inhomogeneous broadening. We used electron beam lithography to pattern arrays of nanobeam cavities attached to large square pads from one side and have free tapered ends from the other side. Hydrofluoric acid solution is then used to remove the AlGaAs sacrificial layer to create a suspended structure, as demonstrated by the scanning electron microscopy (SEM) image shown in Fig. 2(a). The structure consists of three nanobeam cavities attached to a $30 \times 30\,\mu\mathrm{m}^2$ pad region.

In the second part of the fabrication process, we used a $30 \times 30 \times 40\,\mu\mathrm{m}^3$ polydimethylsiloxane (PDMS) stamp to pick-and-place the nanobeam arrays via the square pad.[24–26] After removing the nanobeam arrays from the GaAs substrate, we transfer-printed them onto the edge of a silicon carrier chip. Figure 2(b) shows an SEM image of the finalized device with arrays of nanobeam cavities suspended from the edge of the carrier chip. This method enables nanobeam

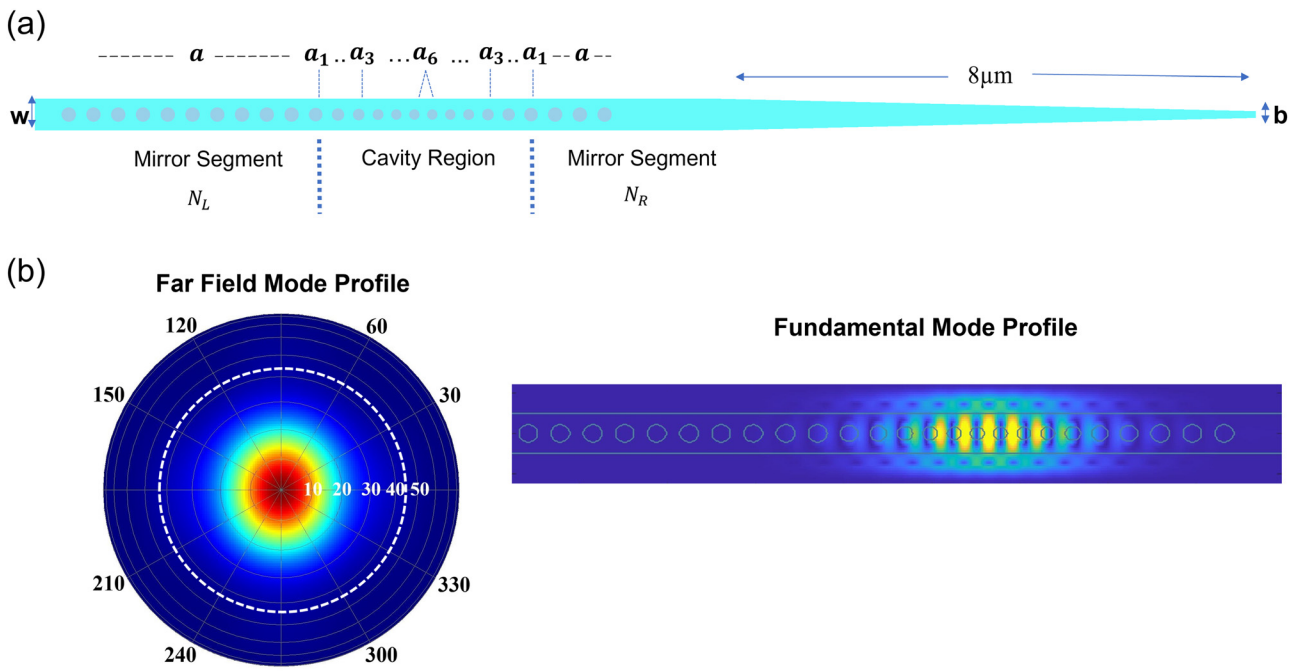

FIG. 1. (a) The tapered nanobeam photonic crystal cavity design with lattice parameter $a = 365$ nm, hole radius $r = 0.29\,a$, and $r_{1,6} = 0.29\,a_{1,6}$. The number of holes in the mirror segments on the right and left sides is $N_R = 4$ and $N_L = 9$, respectively. The cavity region is realized by tapering and shifting 12 holes located between two mirror segments. The width of the nanobeam waveguide is $w = 480$ nm, and the width of taper end is $b = 150$ nm. Nanobeam width is adiabatically reduced from 480 to 150 nm at the end of the 8 μm-long taper. Thickness of the nanobeam is 200 nm. (b) The far field mode profile from the nanobeam taper and fundamental mode profile of the cavity are shown here. White dashed line in far field profile corresponds to numerical aperture of 0.7 of the objective lens.

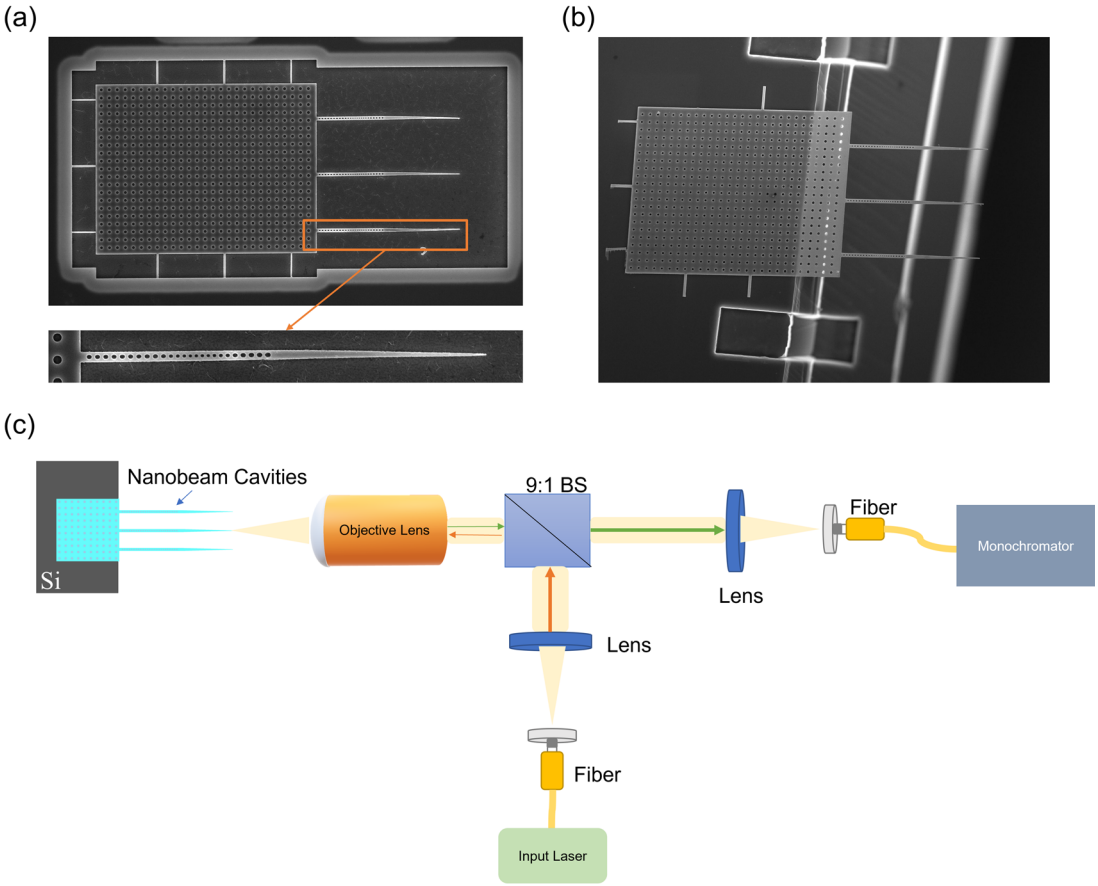

FIG. 2. (a) SEM image of a nanobeam array, attached to a pad that is suspended with support bridges. (b) SEM image of the transferred nanobeam array, suspended at the edge of a silicon carrier chip. (c) A schematic of the measurement setup for the transferred nanobeam array.

waveguides to be efficiently edge-coupled to the objective lens from the tapered side. It also provides our device an easy way for rapid integration with other photonic circuits.

Figure 2(c) shows the experimental setup for the suspended nanobeam photonic crystal cavities. We used a linearly polarized tunable continuous wave (CW) laser and couple it into the tapered side of the suspended nanobeams using an objective lens with an NA of 0.7. Reflected light is collected back with a 9:1 beam splitter (BS) and then detected in a monochromator with a InGaAs detector. Using this setup, we first characterized nanobeam cavities and selected one with fundamental mode at 1284.5 nm with a quality factor of 2830, as shown in the supplementary material, Fig. S1. After carefully aligning optical coupling into the nanobeam cavity, we injected the CW laser off-resonantly to the nanobeam cavities to derive the coupling efficiency. Reflected light from off-resonant laser is measured before the monochromator. After taking into account for efficiency of each optic on the optical path before the nanobeam taper, the coupling efficiency is calculated from ratio of total reflected and injected optical power between nanobeam cavity and the objective lens, where off-resonant reflectance from nanobeam cavity is taken to be unity from FDTD simulations.[27] From these calculations, the coupling efficiency into the nanobeam waveguide from the objective lens was found to be 30%. We attribute the difference between the measured and simulated coupling efficiency (>90%) to the angular alignment of the transferred nanobeams relative to optical axis of the objective lens, and in addition, the scattering losses from the outcoupling nanobeam tapers.

Figure 3 shows the cavity reflectivity spectrum when incident light is scanned from shorter wavelengths to longer wavelengths at various excitation powers using the continuous wave laser. For the scan at a power of 6 μW, we see a symmetric dip of the cavity resonance at 1284.5 nm, consistent with the photoluminescence spectrum of the cavity shown in Fig. S1 in the supplementary material. When we increase the power of the incident laser to 15 μW, we observed that the cavity resonance red shifts and the reflected light spectrum becomes asymmetric. The shift increases with increasing laser power, which is a strong indication of a thermo-optic red shift due to absorption inside the cavity.[12–18,28–30] The asymmetry in the cavity reflectivity is explained by the fact that when we scan the wavelength of the incident laser from the shorter wavelengths toward the cavity resonance, the cavity starts to absorb more light. This increased absorption causes a red shift of cavity resonance away from the laser wavelength due to thermo-optic effect. The red shift of the cavity resonance produces a long tail toward shorter wavelengths in the reflectivity spectrum until the wavelength of the laser scan becomes resonant with the

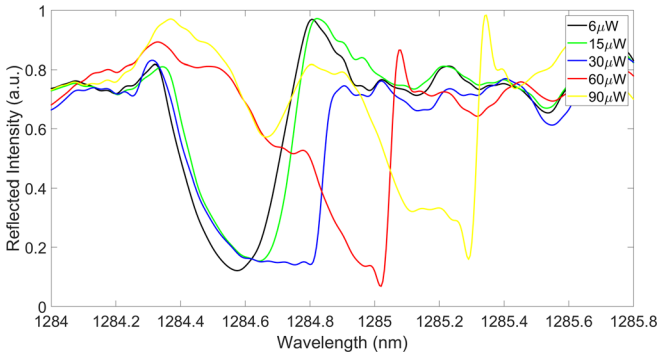

FIG. 3. The reflected intensity from the cavity as the wavelength of the incident CW laser is scanned across the cavity resonance at different power levels.

cavity, and absorption reaches its maximum value. At this point, when the laser is tuned further red, the resonance with the cavity is lost, and the absorption from the laser sharply decreases. As the wavelength of incident light moves away from the cavity, the cavity resonance starts to blue shift back toward the initial cavity resonance due to rapidly decreasing absorption inside the cavity. At high power levels, this sudden loss of resonance and absorption is strong enough to sharply retune the cavity back to the initial resonance and cause strong asymmetry in the reflectivity spectrum.

To investigate the bistable hysteresis response of reflected light from the cavity, we set the laser wavelength at a fixed detuning of $\boldsymbol{\delta}$ from the cavity resonance, as shown in Fig. 4, and sweep the laser power. Figure 4(a) shows the cavity reflectivity as we sweep incident laser power with $\boldsymbol{\delta} = 0$ from low to high power (red curve) and high to low power (blue curve). In the resonant ($\boldsymbol{\delta} = 0$) case, incident laser and cavity mode are fully overlapped, and reflected light is at the lowest reflectivity value from the cavity spectrum. As we increase the power, the cavity starts to thermo-optically red shifts away from the laser wavelength and the reflectivity increases slowly. When we decrease the laser power, the reflectivity follows back the same path to the initial position. We do not observe any difference in optical response for increasing and decreasing laser power.

Figures 4(b)–4(f) show the same measurement when incident laser is further red detuned from the cavity resonance. When the $\boldsymbol{\delta}$ is below 0.4 nm, we observed a strong nonlinear response without any significant difference in increasing and decreasing laser power.

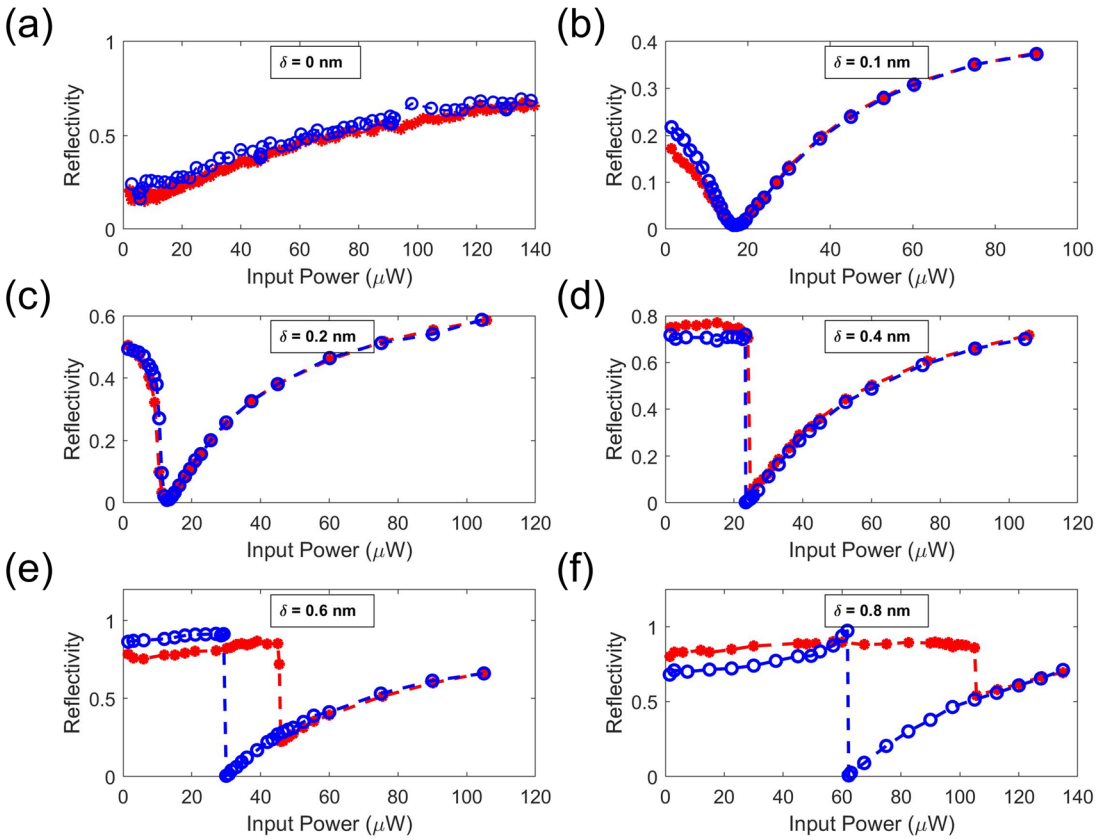

FIG. 4. The cavity reflectivity for input power with different detuning $\boldsymbol{\delta}$ of wavelength of CW laser from wavelength of the cavity resonance. $\boldsymbol{\delta} = \lambda_L - \lambda_c$, where λ_L is the wavelength of incident light and λ_c is the wavelength of the cavity resonance. The red and blue data points represent increasing and decreasing incident power, respectively. (a) $\boldsymbol{\delta} = 0$ nm. CW laser is resonant with the cavity. (b)–(f) $\boldsymbol{\delta}$ is 0.1–0.8 nm, respectively. CW laser is red detuned from the cavity resonance. Input power is measured before the objective lens and adjusted according to coupling efficiency into the nanobeam waveguide.

At 0.4 nm of δ, we start to observe a clear discontinuity and hysteresis that corresponds to optical bistability. Theoretically, the amount of wavelength shift ($\Delta\lambda$) required from the cavity resonance to reach bistable threshold has been shown to be $\Delta\lambda = \frac{\sqrt{3}}{2}\frac{\lambda_c}{Q}$.[18] For this cavity, $\Delta\lambda$ is around 0.39 nm, which explains why hysteresis appears after 0.4 nm of δ. Power threshold for reaching the bistable region is 23 μW with 6.02 dB response contrast between upper and lower states in the middle of hysteresis. Further increasing detuning of incident light to 0.6 and 0.8 nm results in a broadened hysteresis and requires a higher power threshold of 45 μW and 107 μW to reach the bistable region, respectively. Increasing power beyond the bistable region further red shifts the cavity away from the laser. However, with less overlap between the cavity mode and the laser mode, the change in the reflectivity slows down at higher power levels.

To determine whether the bistability is provided by the quantum dot absorption, we also performed similar measurements on an identical device that did not contain quantum dots, as shown in the supplementary material, Fig. S2. In this case, we did not observe an optical bistability and obtained a completely linear relation between the incident and reflected power. This measurement strongly indicates that the cause of optical absorption and the thermo-optic effect is due to quantum dots rather than other mechanisms such as two photon absorption in the GaAs waveguide.

In conclusion, we have demonstrated room-temperature, thermally induced optical bistability at telecom wavelengths using quantum dots embedded in a nanobeam photonic crystal cavity. We can achieve bistable thresholds as low as 23 μW, which is more than an order of magnitude lower than previous quantum-dot-based devices[8,12] while having a large operation bandwidth due to the moderate quality factor of the cavity. Nanobeam photonic crystal cavity designs with high transmissions and moderate quality factors have also been demonstrated before.[31,32] These designs could be incorporated with our approach to realize air-suspended cavities that are adiabatically coupled into silicon photonic circuits using transfer-printing methods.[24–26] Moreover, the thermo-optical nature of the bistability in our device can be used to realize low-power thermal memories[16,33] and nonlinear optical activation functions.[34] Our device is promising for many photonic applications that require hybrid-integrated low-power optical nonlinearities at telecom wavelengths.

See the supplementary material for further characterization measurements for the nanobeam photonic crystal cavity and input–output measurements for nanobeam photonic crystal cavities without quantum dots.

The authors acknowledge support from the National Science Foundation (Grant Nos. OMA1936314 and ECCS1933546), the Army Research Office (Grant No. W911NF1910378), the Office of Naval Research (Grant No. N000142012551), the Air Force Office of Scientific Research (Grant No. FA23862014072), the Maryland-ARL Quantum Partnership, and the Laboratory for Telecommunication Sciences.

AUTHOR DECLARATIONS

Conflict of Interest

The authors have no conflicts to disclose.

Author Contributions

Mustafa Atabey Buyukkaya: Conceptualization (lead); Data curation (lead); Formal analysis (lead); Investigation (lead); Methodology (lead); Software (lead); Validation (lead); Visualization (lead); Writing – original draft (lead); Writing – review and editing (lead). **Chang-Min Lee:** Methodology (supporting); Software (supporting). **Ahmad Mansoori:** Resources (supporting). **Ganesh Balakrishnan:** Resources (supporting). **Edo Waks:** Funding acquisition (lead); Investigation (supporting); Methodology (supporting); Resources (supporting); Supervision (equal); Writing – review and editing (equal).

DATA AVAILABILITY

The data that support the findings of this study are available within the article and its supplementary material.

REFERENCES

[1]H. Gibbs, *Optical Bistability: Controlling Light With Light* (Elsevier, 2012).
[2]T. Tanabe, M. Notomi, S. Mitsugi, A. Shinya, and E. Kuramochi, Opt. Lett. **30**, 2575 (2005).
[3]E. Kuramochi, K. Nozaki, A. Shinya, K. Takeda, T. Sato, S. Matsuo, H. Taniyama, H. Sumikura, and M. Notomi, Nat. Photonics **8**, 474 (2014).
[4]A. Hurtado, I. D. Henning, and M. J. Adams, Appl. Phys. Lett. **91**, 151106 (2007).
[5]T. Alexoudi, G. T. Kanellos, and N. Pleros, Light. Sci. Appl. **9**, 91 (2020).
[6]Q. M. Ngo, K. Q. Le, D. L. Vu, and V. H. Pham, J. Opt. Soc. Am. B **31**, 1054 (2014).
[7]M.-K. Kim, I.-K. Hwang, S.-H. Kim, H.-J. Chang, and Y.-H. Lee, Appl. Phys. Lett. **90**, 161118 (2007).
[8]C. Arnold, V. Loo, A. Lemaître, I. Sagnes, O. Krebs, P. Voisin, P. Senellart, and L. Lanco, Appl. Phys. Lett. **100**, 111111 (2012).
[9]Q. Xu and M. Lipson, Opt. Lett. **31**, 341 (2006).
[10]L. Zhang, L. Zhan, M. Qin, Z. Zou, Z. Wang, and J. Liu, J. Opt. Soc. Am. B **32**, 1113 (2015).
[11]X. C. Jiang, Y. W. Zhou, D. L. Gao, Y. Huang, and L. Gao, Opt. Express **28**, 17384 (2020).
[12]M. Brunstein, R. Braive, R. Hostein, A. Beveratos, I. Rober-Philip, I. Sagnes, T. J. Karle, A. M. Yacomotti, J. A. Levenson, V. Moreau, G. Tessier, and Y. De Wilde, Opt. Express **17**, 17118 (2009).
[13]F. Ramiro-Manzano, N. Prtljaga, L. Pavesi, G. Pucker, and M. Ghulinyan, Opt. Lett. **38**, 3562 (2013).
[14]R. Shankar, I. Bulu, R. Leijssen, and M. Lončar, Opt. Express **19**, 24828 (2011).
[15]M. Clementi, S. Iadanza, S. A. Schulz, G. Urbinati, D. Gerace, L. O'Faloain, and M. Galli, Light. Sci. Appl. **10**, 240 (2021).
[16]A. M. Morsy, R. Biswas, and M. L. Povinelli, APL Photonics **4**, 010804 (2019).
[17]K. Perrier, S. Greveling, H. Wouters, S. R. K. Rodriguez, G. Lehoucq, S. Combrié, A. de Rossi, S. Faez, and A. P. Mosk, OSA Continuum **3**, 1879 (2020).
[18]L.-D. Haret, T. Tanabe, E. Kuramochi, and M. Notomi, Opt. Express **17**, 21108 (2009).
[19]J. B. Khurgin, G. Sun, W. T. Chen, W.-Y. Tsai, and D. P. Tsai, Sci. Rep. **5**, 17899 (2015).
[20]S. W. Osborne, P. Blood, P. M. Smowton, Y. C. Xin, A. Stintz, D. Huffaker, and L. F. Lester, J. Phys.: Condens. Matter **16**, S3749 (2004).
[21]Y. Gong, B. Ellis, G. Shambat, T. Sarmiento, J. S. Harris, and J. Vuckovic, Opt. Express **18**, 8781 (2010).
[22]R. Ohta, Y. Ota, M. Nomura, N. Kumagai, S. Ishida, S. Iwamoto, and Y. Arakawa, Appl. Phys. Lett. **98**, 173104 (2011).
[23]S. A. Moore, L. O'Faolain, M. A. Cataluna, M. B. Flynn, M. V. Kotlyar, and T. F. Krauss, IEEE Photonics Technol. Lett. **18**, 1861 (2006).
[24]J. Zhang, G. Muliuk, J. Juvert, S. Kumari, J. Goyvaerts, B. Haq, C. Op de Beeck, B. Kuyken, G. Morthier, D. Van Thourhout, R. Baets, G. Lepage, P. Verheyen, J. Van Campenhout, A. Gocalinska, J. O'Callaghan, E. Pelucchi, K. Thomas, B. Corbett, A. J. Trindade, and G. Roelkens, APL Photonics **4**, 110803 (2019).

[25]J. Lee, I. Karnadi, J. T. Kim, Y.-H. Lee, and M.-K. Kim, ACS Photonics **4**, 2117 (2017).
[26]R. Katsumi, Y. Ota, A. Osada, T. Yamaguchi, T. Tajiri, M. Kakuda, S. Iwamoto, H. Akiyama, and Y. Arakawa, APL Photonics **4**, 036105 (2019).
[27]M. J. Burek, C. Meuwly, R. E. Evans, M. K. Bhaskar, A. Sipahigil, S. Meesala, B. Machielse, D. D. Sukachev, C. T. Nguyen, J. L. Pacheco, E. Bielejec, M. D. Lukin, and M. Lončar, Phys. Rev. Appl. **8**, 024026 (2017).
[28]T. Gu, M. Yu, D.-L. Kwong, and C. W. Wong, Opt. Express **22**, 18412 (2014).
[29]Y. Gao, W. Zhou, X. Sun, H. K. Tsang, and C. Shu, Opt. Lett. **42**, 1950 (2017).
[30]S. Iadanza, M. Clementi, C. Hu, S. A. Schulz, D. Gerace, M. Galli, and L. O'Faolain, Phys. Rev. B **102**, 245404 (2020).
[31]Q. Quan and M. Loncar, Opt. Express **19**, 18529 (2011).
[32]M. W. McCutcheon, P. B. Deotare, Y. Zhang, and M. Lončar, Appl. Phys. Lett. **98**, 111117 (2011).
[33]C. Khandekar and A. W. Rodriguez, Appl. Phys. Lett. **111**, 083104 (2017).
[34]B. Wu, H. Li, W. Tong, J. Dong, and X. Zhang, Opt. Mater. Express **12**, 970 (2022).